Am J Clin Exp Urol 2026;14(5):189-203
www.ajceu.us /ISSN:2330-1910/AJCEU0172099

Original Article

Multi-omics analysis identified ASRGL1 as a novel oncogene and potential therapeutic target in prostate cancer

Yuan Ma[1*], Rong Fan[2*], Wenyue Yu[3*], Kefei Duan[4*], Gaoteng Lin[2], Zheng Chen[2], Guizhong Li[1]

[1]Department of Urology, Beijing Jishuitan Hospital, Capital Medical University, Beijing 100035, China; [2]Department of Urology, The First Affiliated Hospital of Jinan University, Guangzhou 510630, Guangdong, China; [3]Department of Urology, General Hospital of Southern Theater Command, Guangzhou 510000, Guangdong, China; [4]Department of Cerebrovascular Diseases, Beijing Anzhen Hospital, Capital Medical University, Beijing 100029, China. [*]Equal contributors.

Received February 13, 2026; Accepted September 23, 2026; Epub October 25, 2026; Published October 30, 2026

Abstract: Background: Prostate Cancer (PCa) is a globally prevalent malignancy with high heterogeneity and frequent therapy resistance. Identifying novel causal drivers and understanding their roles in the tumor microenvironment (TME) are crucial for developing new therapeutic strategies. Methods: We employed an integrative multi-omics approach. First, we analyzed single-cell RNA sequencing (scRNA-seq) data from prostate tissues to identify differentially expressed genes. Mendelian Randomization (MR) analysis was then performed using cis-expression quantitative trait loci (cis-eQTLs) and cis-protein QTLs (cis-pQTLs) from the deCODE database to infer causal relationships between gene/protein expression and PCa risk. Findings were validated using bulk transcriptomic and clinical data from The Cancer Genome Atlas (TCGA) cohort. Functional enrichment, immune microenvironment analysis, and drug sensitivity profiling were conducted to elucidate the oncogenic mechanisms of the candidate gene. Results: MR analysis identified asparaginase-like 1 (ASRGL1) as a novel causal risk factor for PCa (OR = 1.074, 95% CI: 1.032-1.118, P < 0.001). Consistently, ASRGL1 expression was significantly upregulated in PCa tumors and associated with poor patient prognosis. scRNA-seq analysis revealed that ASRGL1 was predominantly expressed in mast cells within the TME. Functional studies indicated that high ASRGL1 expression correlated with activated cell cycle pathways, dysregulated cholesterol homeostasis, and an immunosuppressive TME. Furthermore, we identified several potential therapeutic compounds (e.g., panobinostat, pevonedistat) that showed predicted efficacy against ASRGL1-high PCa models. Conclusion: Our study establishes ASRGL1 as a causal oncogene in PCa, linking its expression to mast cell function, metabolic reprogramming, and immune suppression. These findings nominate ASRGL1 as a promising prognostic biomarker and a potential therapeutic target, offering new insights for PCa treatment.

Keywords: Single-cell RNA sequencing, Mendelian randomisation, asparaginase-like 1 gene, tumor microenvironment, prostate cancer

Introduction

Prostate cancer (PCa) has emerged as the most prevalent malignant tumor among men worldwide, imposing a substantial global health burden. According to the latest GLOBOCAN statistics, PCa accounted for 1.46 million new cases in 2022, representing 14.5% of all newly diagnosed malignancies in males [1]. Driven by population aging this figure is projected to exceed 2.9 million by 2040, accompanied by a continuous rise in mortality rates [2, 3]. Despite the widespread adoption of prostate-specific antigen (PSA)-based screening, which has improved early detection, the clinical management of PCa remains fraught with challenges, including overdiagnosis, overtreatment, and the inevitable development of resistance to standard therapies [4, 5]. The etiology of PCa is multifactorial, involving a complex interplay of genetic predisposition, hormonal regulation, chronic inflammation, and epigenetic alterations. At the genetic level, high-penetrance mutations (e.g., BRCA2, HOXB13) and numerous low-penetrance susceptibility loci identified via genome-wide association studies (GWAS)

https://doi.org/10.62347/BUMQ2278

collectively shape an individual's baseline risk [6]. Hormonally, androgens - particularly dihydrotestosterone (DHT) - serve as the primary drivers of prostatic carcinogenesis. By binding to the androgen receptor (AR), DHT activates transcriptional programs that promote cell proliferation and inhibit apoptosis. Chronic prostatic inflammation, often triggered by infections or dietary factors (e.g., high-fat diets), further exacerbates genomic instability through the generation of reactive oxygen species, thereby facilitating tumor initiation [7]. Concurrently, epigenetic modifications, such as aberrant DNA methylation (e.g., silencing of the tumor suppressor GSTP1) and histone modifications, occur early in disease development, contributing to the malignant phenotype.

The clinical trajectory of PCa is highly heterogeneous, necessitating risk-adaptive treatment strategies. For localized disease, management hinges on risk stratification. Low-risk patients are typically candidates for active surveillance, a strategy designed to monitor indolent disease via serial PSA testing, digital rectal examinations, and repeat biopsies, thereby deferring curative intervention and avoiding treatment-related morbidities such as urinary incontinence and erectile dysfunction [8, 9]. Conversely, intermediate-to-high-risk localized PCa is primarily managed with curative intent through radical prostatectomy or radiotherapy (including intensity-modulated radiation therapy and brachytherapy). While these modalities offer excellent cancer-specific survival for organ-confined disease, biochemical recurrence occurs in approximately 20-30% of patients, signaling the persistence of micrometastatic disease or the emergence of treatment-resistant clones [8, 9].

For advanced or metastatic PCa, the cornerstone of treatment is androgen deprivation therapy (ADT) and next-generation AR pathway inhibitors (e.g., enzalutamide, abiraterone). However, nearly all patients eventually progress to castration-resistant prostate cancer (CRPC), a lethal phenotype driven by mechanisms such as AR amplification, splice variants (e.g., AR-V7), and ligand-independent AR activation [10, 11]. Furthermore, the efficacy of emerging immunotherapies remains limited in PCa, largely attributable to an immunosuppressive tumor microenvironment (TME) characterized by paucity of effector T cells, abundance of cancer-associated fibroblasts (CAFs), and dysregulated stromal-immune crosstalk [7, 12].

Current therapeutic limitations underscore the urgent need to dissect the molecular underpinnings of PCa progression and therapy resistance. While GWAS have successfully mapped thousands of risk loci, the majority reside in non-coding regions, obscuring their functional impact on target genes and proteins. Integrating single-cell transcriptomics with Mendelian randomization (MR) offers a powerful solution to bridge this gap. Single-cell RNA sequencing (scRNA-seq) resolves the cellular and molecular architecture of the TME at unprecedented resolution, while MR leverages genetic variation as instrumental variables to infer causality between molecular phenotypes (e.g., gene/protein expression) and disease risk, effectively circumventing confounding biases inherent to observational studies [13].

In this study, we integrated scRNA-seq atlases, cis-expression quantitative trait loci (cis-eQTL), cis-protein quantitative trait loci (cis-pQTL), and bulk RNA-seq data from The Cancer Genome Atlas (TCGA) to systematically identify and validate novel drivers of PCa. Our multi-omics analytical framework specifically focuses on deciphering the role of the asparaginase-like 1 (ASRGL1) gene. We elucidate how ASRGL1 contributes to PCa pathogenesis through the regulation of cholesterol homeostasis, cell cycle progression, and the remodeling of the immunosuppressive TME, thereby identifying it as a promising prognostic biomarker and therapeutic target.

Methods

Genome-wide association study (GWAS) data

Summary statistics for PCa were obtained from the IEU Open GWAS project (https://gwas.mrcieu.ac.uk/) under accession ebi-a-GCST006085. This dataset was selected because it represents one of the largest and most recent GWAS meta-analyses for prostate cancer in individuals of European ancestry, providing robust statistical power for MR analysis. The dataset includes 140,254 individuals (79,148 cases and 61,106 controls) of European descent. Only summary-level data for the PCa phenotype were downloaded. No individual-level genotype or phenotype filtering was performed by the authors, as the analysis used publicly available summary statistics.

Single-cell RNA sequencing (scRNA-seq) data

In this study, the scRNA-seq dataset GSE-193337 was downloaded from the Gene Expression Omnibus (GEO) database. This dataset was specifically chosen because it contains paired prostate tissue samples from four PCa patients and four healthy donors, enabling a direct and matched comparison of the TME cellular landscape against normal tissue.

Post-download, standard quality control (QC) was applied at the cell level using the Seurat package (v4.0.2). Cells were retained if they met the following criteria: (1) expression between 200 and 5,000 genes, and (2) had a mitochondrial gene content percentage below 20%. Genes detected in fewer than 3 cells were filtered out. This QC process ensured the analysis was based on high-quality, viable single-cell transcriptomes.

We employed the Scale-Controlled Transformation (SCT) method to normalize the data and correct for batch effects across samples. Dimensionality reduction was then performed via Principal Component Analysis (PCA), with the number of principal components set to 50, to capture the major sources of variation in the dataset and to simplify downstream analysis. Subsequently, the Uniform Manifold Approximation and Projection (UMAP) technique was applied to visualize the reduced dimensions and the resulting cell clusters. Finally, cell types were comprehensively annotated based on established cell type-specific surface marker genes.

Bulk transcriptome and clinical data

RNA-seq expression data (FPKM-UQ) and corresponding clinical information for Prostate Adenocarcinoma (PRAD) were retrieved from TCGA (https://www.cancer.gov/tcga) via the Genomic Data Commons (GDC) portal. TCGA-PRAD is the largest and most comprehensive publicly available cohort for PCa, providing the necessary sample size for survival, differential expression, and immune infiltration analyses. Only primary tumor samples (sample_type.samples = "Primary Tumor") and solid tissue normal samples (sample_type.samples = "Solid Tissue Normal") from the PRAD project were included. Samples with missing overall survival (OS) or progression-free interval (PFI) data were excluded from the respective survival analyses. This resulted in a final cohort of 490 primary tumor samples and 52 adjacent normal samples for expression comparison.

Gene set enrichment analysis (GSEA) was performed to identify significantly enriched biological pathways. The analysis utilized gene sets from the Kyoto Encyclopedia of Genes and Genomes (KEGG) and Gene Ontology (GO) databases, which were obtained from the Molecular Signature Database (MSigDB; files: "c2.cp.kegg.v2022.1.Hs.symbols.gmt" and "c5.go.v2022.1.Hs.symbols.gmt"). Enrichment computations were carried out using the clusterProfiler and GSEA packages in R. Additionally, single-sample GSEA (ssGSEA) was conducted to quantify immune cell infiltration levels in each sample.

MR studies using cis-eQTL as IVs for differential gene expression

In the single-cell data analysis, we identified 1,761 differentially expressed genes. For each gene, we conducted cis-eQTL analysis, identifying 134 genes with potential causal associations with prostate cancer.

Plasma protein quantitative trait loci (pQTL) data

Genetic instruments for plasma protein levels were derived from pQTL study by Ferkingstad et al (2021). This study was selected as it constitutes the largest-to-date GWAS of the plasma proteome, measuring 4,179 proteins in 35,559 Icelandic individuals, offering extensive coverage for cis-pQTL discovery. For each protein of interest, we extracted cis-pQTLs (single nucleotide polymorphisms, SNPs, located within ± 1 Mb of the protein-coding gene) that were associated with protein abundance at a genome-wide significance level ($P < 5\times10^{-8}$). Only independent SNPs (linkage disequilibrium, LD, $r^2 < 0.05$ within a 10,000 kb window) were used as instrumental variables (IVs) in the MR analysis to ensure independence and avoid bias from correlated genetic variants.

Sensitivity analyses for multi-IV exposure variables

We performed comprehensive sensitivity analyses to assess the robustness of the MR esti-

mates. For exposure variables instrumented by multiple SNPs, we evaluated heterogeneity across variant-specific estimates using the mr_heterogeneity function from the TwoSampleMR package. The potential for horizontal pleiotropy was examined using MR-Egger regression, which provides a test for directional pleiotropy via its intercept term. Exposure variables with a statistically significant MR-Egger intercept (*P*-value < 0.05) were considered to have potential pleiotropic bias and were subsequently excluded. To further ensure that the overall causal estimate was not disproportionately driven by any single genetic variant, we conducted a leave-one-out sensitivity analysis for exposures with more than two instrumental variables. This involved iteratively removing each SNP and recalculating the MR estimate with the remaining set.

Statistical analysis

All statistical analysis was conducted in R (Version 4.1.2). Associations between two continuous variables were assessed using Pearson's or Spearman's correlation analyses as appropriate. Survival outcomes were analyzed using the Kaplan-Meier method, and differences between groups were compared with the log-rank test. A two-sided *P*-value of less than 0.05 was considered statistically significant for all tests unless otherwise specified.

Results

Single-cell transcriptomic landscape of normal and cancerous human prostate tissue

Single-cell transcriptome sequencing (scRNA-seq) data from four tumor and four benign samples were utilized to delineate the single-cell transcriptome landscape of the human prostate. Following stringent quality control measures, cells with mitochondrial gene content less than 20% and expressing between 200 and 5000 genes were retained. Notably, clear cell clusters were evident in the Uniform Manifold Approximation and Projection (UMAP) visualization (**Figure 1A**, **1B**). After standardized quality control and UMAP clustering, all single cells were annotated into nine subtypes: epithelial cells, CD3+ T cells, B cells, macrophages, mast cells, endothelial cells, fibroblasts, smooth muscle cells and myeloid dendritic cells (**Figure 1D**). The Wilcoxon rank-sum test was used to quantify cell proportion differences between tumor and normal groups ($P < 0.05$). Mast cells, T cells, tumor epithelial cells, macrophages and myeloid dendritic cells occupied significantly higher proportions in PCa tissues, while B cells, smooth muscle cells, endothelial cells and fibroblasts were enriched in benign prostate samples (**Figure 1C**, **1E**).

Mendelian randomization identifies ASRGL1 as a causal risk gene of PCa

Differentially expressed genes (DEGs) between tumor and normal cell populations were calculated via Seurat FindMarkers function with fixed statistical cutoffs: absolute $\log_2$(fold change) ≥ 0.25, adjusted false discovery rate (FDR) < 0.01. Under these clear statistical criteria, a total of 1,761 DEGs were screened out across all prostate cell subsets (**Figure 2A**). Cis-eQTL filtering for all 1,761 DEGs generated 134 candidate genes with genome-wide significant genetic variation signals associated with PCa risk ($P < 5\times10^{-8}$). Among these genes, ASRGL1 possessed qualified independent cis-pQTL instrumental SNPs eligible for two-sample MR analysis (**Figure 2B**, **2C**). IVW MR result showed genetically upregulated ASRGL1 protein expression causally increased PCa risk (OR = 1.074, 95% CI: 1.032-1.118, P < 0.001) (**Figure 3D**). Multiple sensitivity tests verified stable causal estimation: 1. Cochran's Q heterogeneity test: Q = 12.46, P = 0.271, no significant heterogeneity across SNPs; 2. MR-Egger regression intercept test: intercept = 0.0012, P = 0.683, no directional horizontal pleiotropy (**Figure 3C**); 3. Leave-one-out analysis: sequential removal of each SNP generated OR values ranging from 1.061 to 1.087, all 95% CIs excluded 1.0 (**Figure 3A**, **3B**, **3E**).

Clinical expression pattern and pathway enrichment signatures of ASRGL1 in TCGA-PRAD cohort

ASRGL1 mRNA abundance was significantly higher in primary tumor samples compared with unpaired normal adjacent tissues (Wilcoxon test, P < 0.001) and paired normal tissues (paired t-test, P < 0.001) (**Figure 4A**, **4B**). Samples were split into high/low subgroups by median ASRGL1 expression for survival analysis. Kaplan-Meier OS comparison showed high ASRGL1 expression correlated with worse sur-

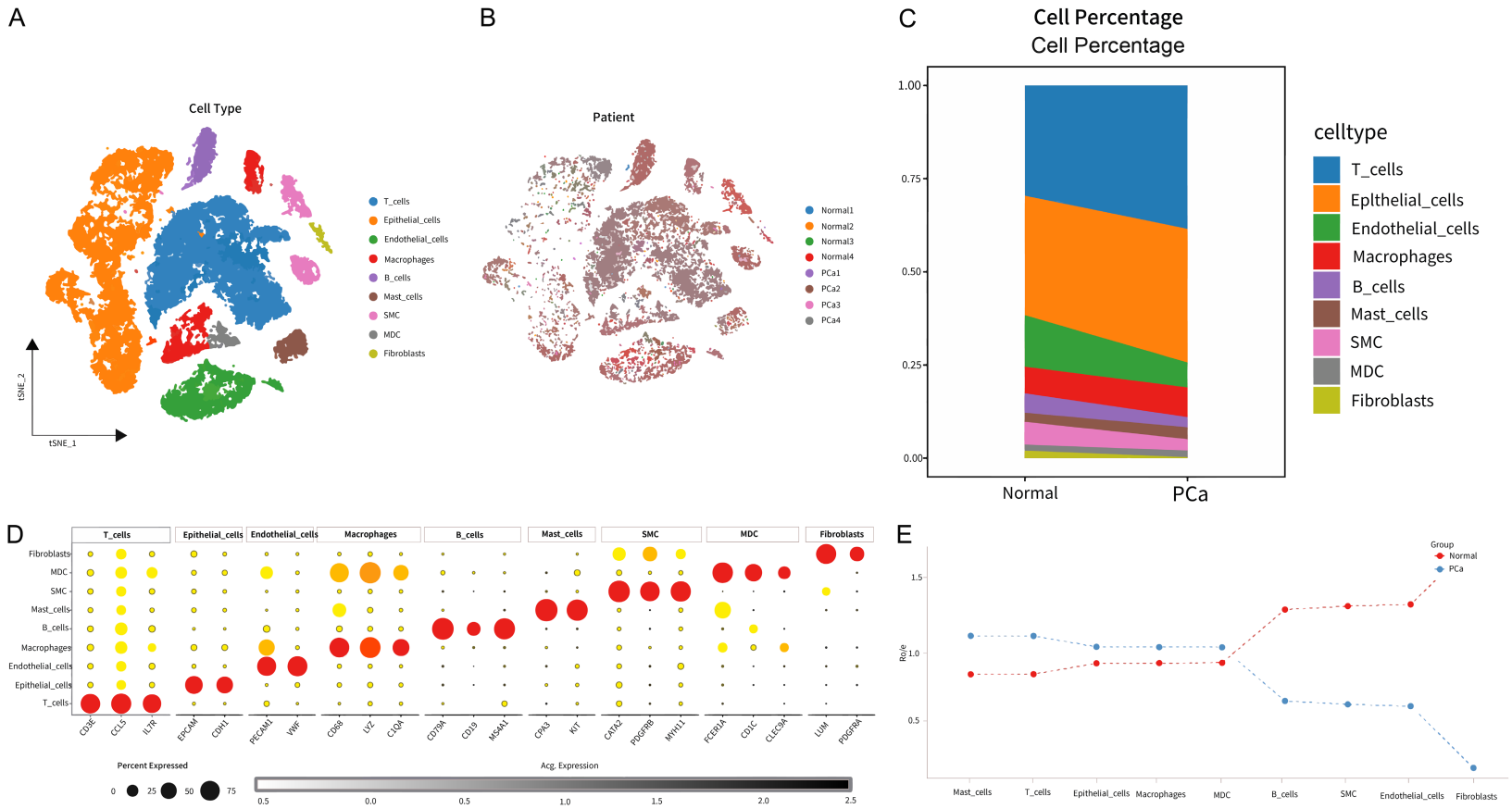


Figure 1. Single-cell transcriptome landscape. A. t-distributed stochastic neighbor embedding (t-SNE) plot colored by cell types. B. t-distributed stochastic neighbor embedding (t-SNE) plot colored by patients. C. Cell percentages in normal and prostate cancer (PCa) samples. D. Dot plot showing gene markers for major cell types. E. Line chart showing Ratio of observed to expected (Ro/e) scores for each cell type.

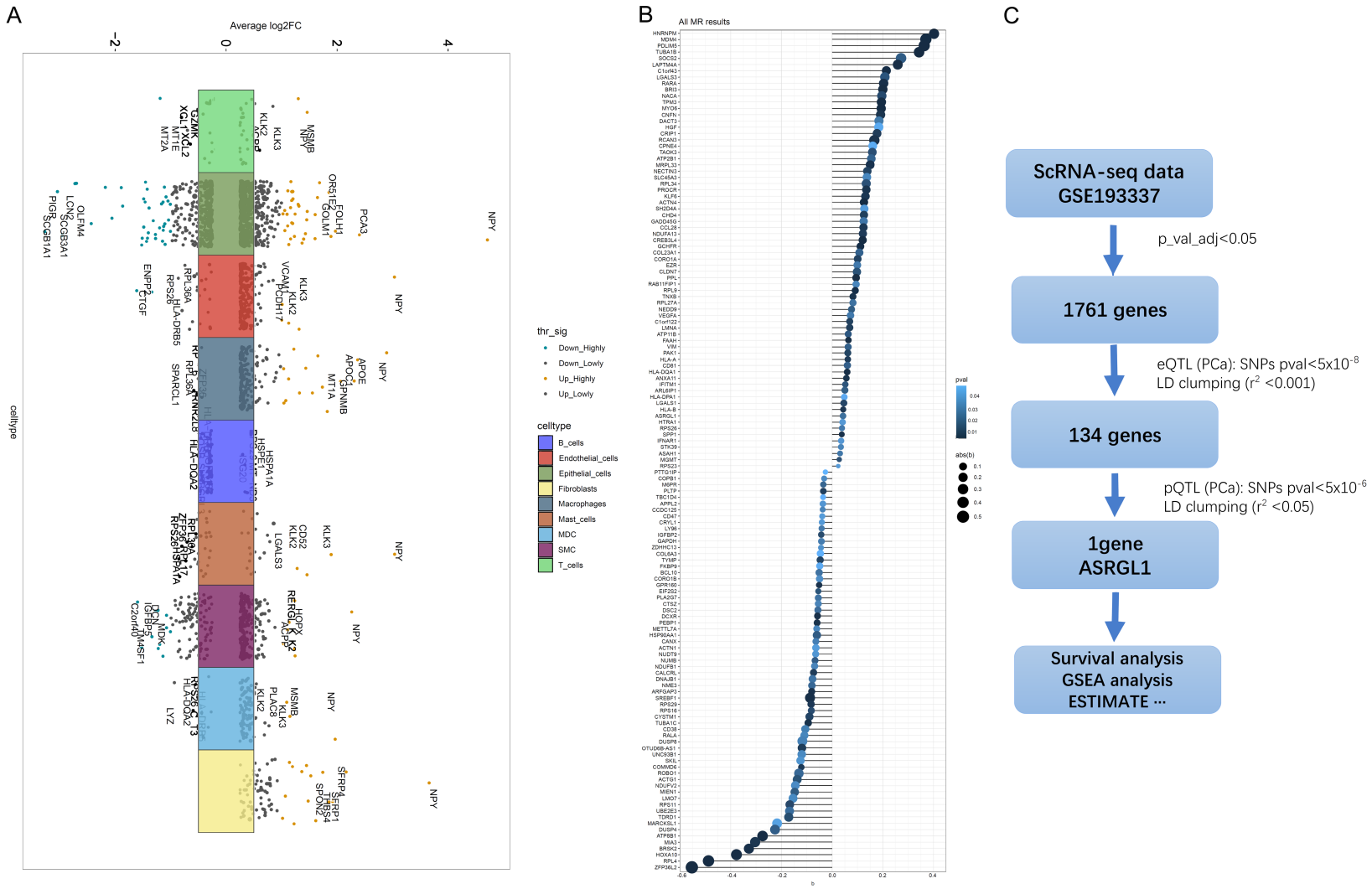


Figure 2. ASRGL1 was identified as a potential oncogene by Mendelian randomization (MR) analysis. A. Differentially expressed genes (DEGs) in major cell types. B. Lollipop chart showing results of MR analysis using cis-expression quantitative trait locus (cis-eQTL) of DEGs. C. Flowchart of the study.

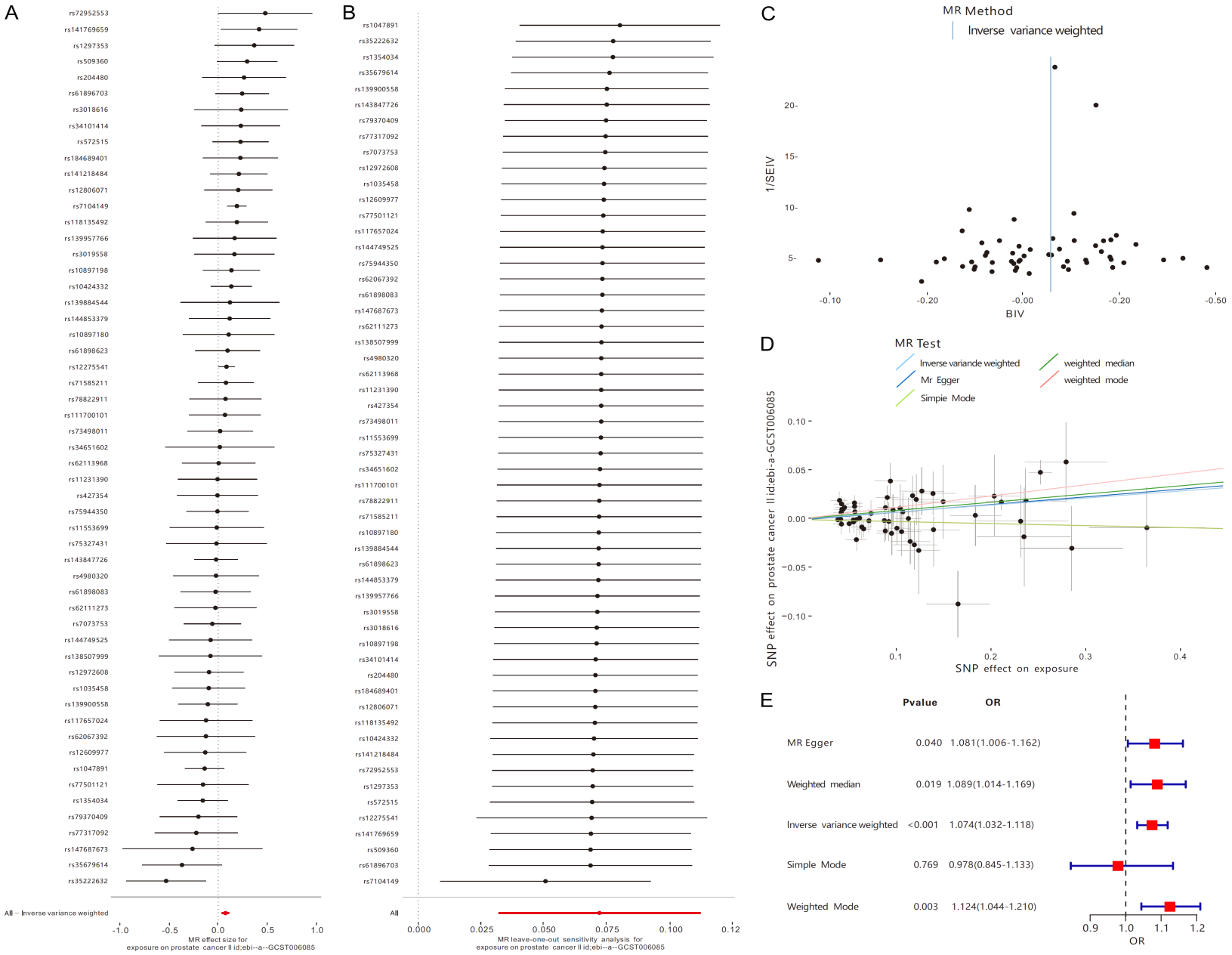

A
B
C
D
E
MR Method
Inverse variance weighted
1/SEIV
BIV
MR Test
Inverse variande weighted
Mr Egger
Simpie Mode
weighted median
weighted mode
SNP effect on prostate cancer II id:ebi-a-GCST006085
SNP effect on exposure
Pvalue
OR
MR Egger 0.040 1.081(1.006-1.162)
Weighted median 0.019 1.089(1.014-1.169)
Inverse variance weighted <0.001 1.074(1.032-1.118)
Simple Mode 0.769 0.978(0.845-1.133)
Weighted Mode 0.003 1.124(1.044-1.210)
OR
All – Inverse variance weighted
MR effect size for exposure on prostate cancer II id:ebi--a--GCST006085
All
MR leave-one-out sensitivity analysis for exposure on prostate cancer II id:ebi--a--GCST006085

Figure 3. The relationship between ASRGL1 and PCa was confirmed by MR analysis. A. Forest plot illustrating MR effect size for ASRGL1 in PCa. B. Forest plot illustrating MR leave-one-out sensitivity analysis for ASRGL1 on PCa. Odds ratios (ORs) and 95% confidence intervals (CIs) are illustrated. C. Funnel plot estimating horizontal pleiotropy of single nucleotide polymorphisms (SNPs). D. Scatter plot showing the SNP effect on prostate cancer. E. Forest plot showing the SNP effect on ASRGL1 and prostate cancer.

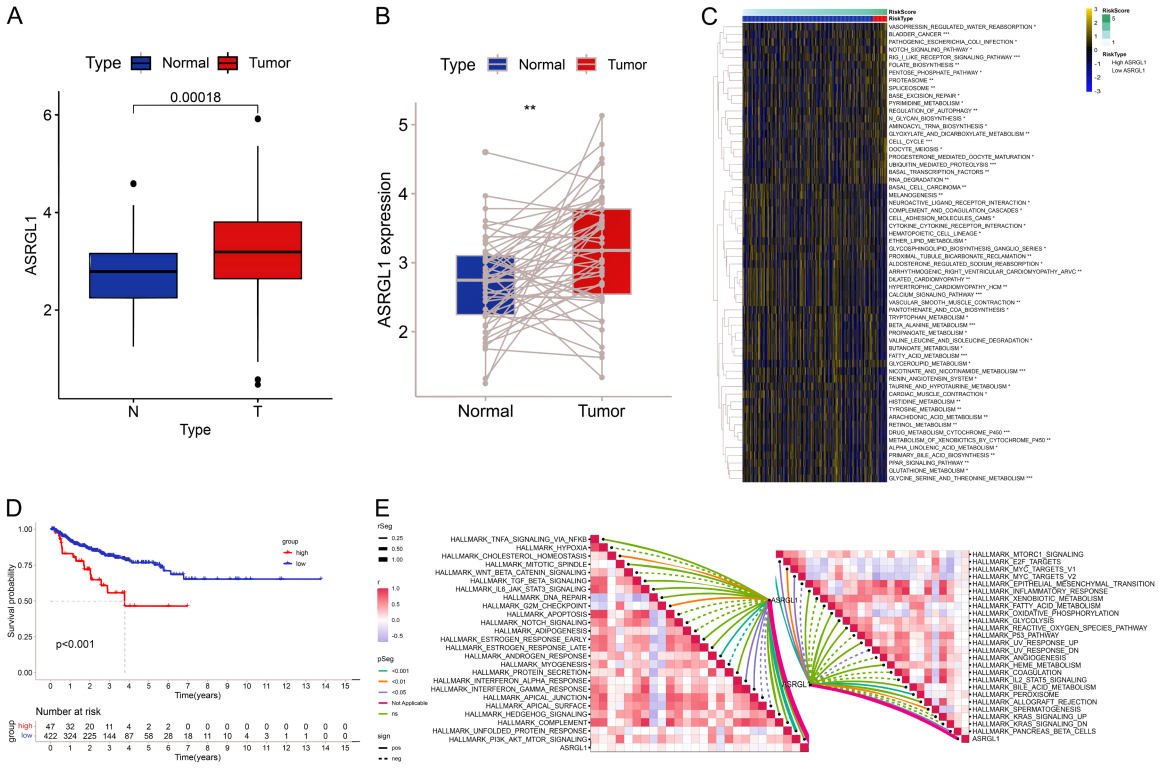


Figure 4. The expression and characteristics of ASRGL1 in PCa. A. Boxplot showing the expression of ASRGL1 in normal and prostate tumor samples. B. Boxplot showing the expression of ASRGL1 in paired normal and tumor prostate samples. C. Heatmap showing the differentially expressed pathways between high- and low-ASRGL1 groups. D. Kaplan-Meier (K-M) plot showing the survival probability in high- and low-ASRGL1 groups. E. Heatmap showing the correlation between ASRGL1 and hallmark pathways.

vival outcome (HR = 1.42, 95% CI: 1.08-1.87, log-rank P = 0.012) (**Figure 4D**). ssGSEA Spearman correlation coefficients (r_s) between ASRGL1 expression and hallmark pathway activity scores were listed below: Positively correlated pathways: PI3K/AKT/mTOR signaling (r_s = 0.31, FDR < 0.001), G2/M cell cycle checkpoint (r_s = 0.36, FDR < 0.001), cholesterol homeostasis (r_s = 0.28, FDR < 0.001), androgen response (r_s = 0.22, FDR < 0.001); Negatively correlated pathways: epithelial-mesenchymal transition (r_s = -0.24, FDR < 0.001), myogenesis (r_s = -0.20, FDR < 0.001) (**Figure 4E**). Global GSEA results displayed pathways significantly enriched in ASRGL1-high tumors (FDR < 0.05): spliceosome (NES = 1.84, FDR = 0.007), proteasome (NES = 1.72, FDR = 0.011), cell cycle (NES = 1.68, FDR = 0.014). Pathways suppressed in ASRGL1-high tumors included fatty acid metabolism (NES = -1.59, FDR = 0.022) and oxidative phosphorylation (NES = -1.53, FDR = 0.030) (**Figure 4C**).

Immune microenvironment features stratified by ASRGL1 expression

ESTIMATE algorithm scores, TIDE scores, cytotoxic marker expression and ssGSEA immune cell infiltration scores were quantified for ASRGL1 high/low subgroups. No statistical difference of ESTIMATE immune score was detected between groups (P = 0.106). The ASRGL1-high subgroup had significantly elevated stromal score (median difference = 0.13, Wilcoxon P = 0.028) and reduced TIDE score (median difference = -0.21, Wilcoxon P = 0.019)

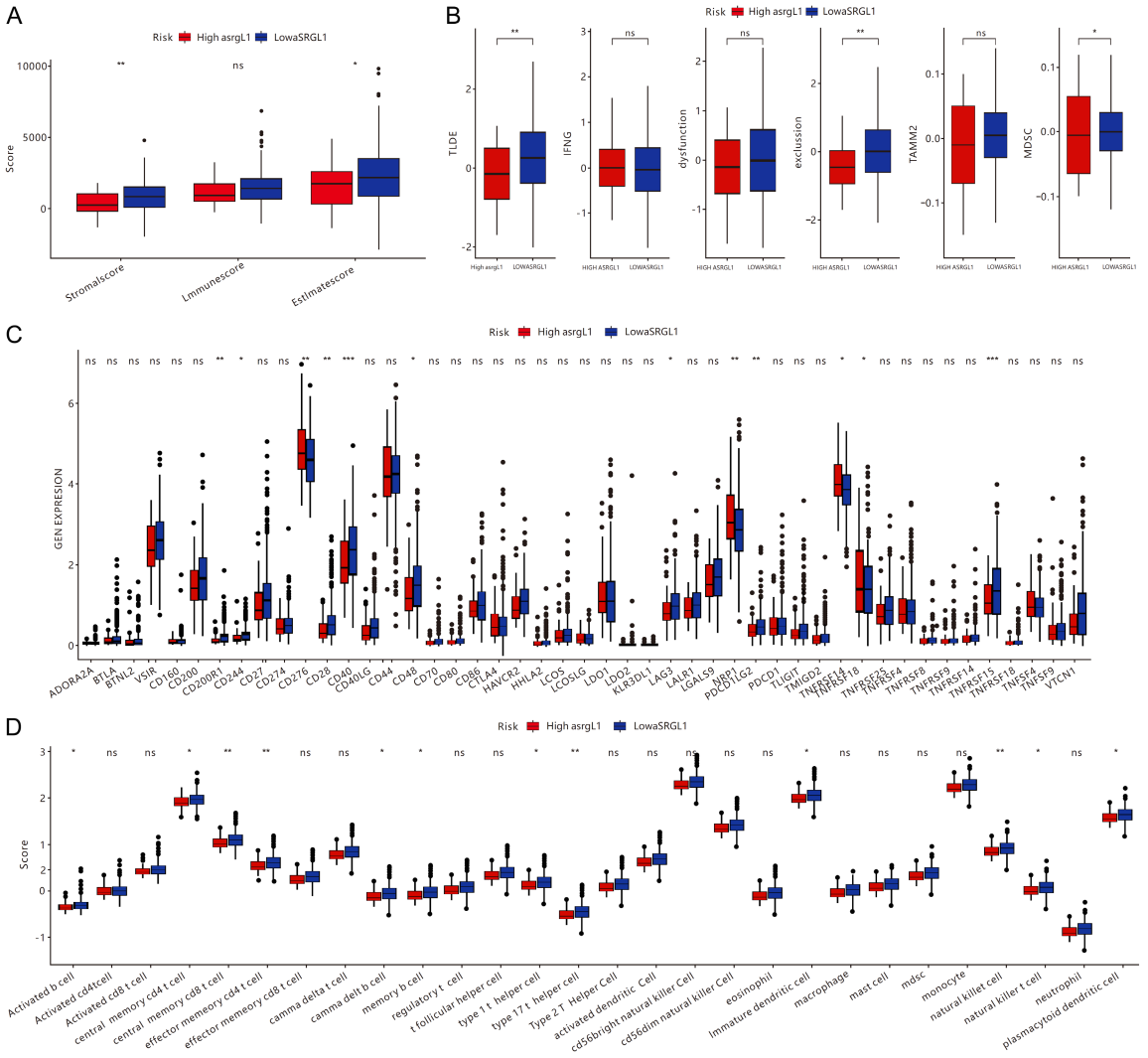


Figure 5. Immune infiltration analysis for ASRGL1. A. Boxplot showing the Estimation of STromal and Immune cells in MAlignant Tumor tissues using Expression data (ESTIMATE) scores in high- and low-ASRGL1 groups. B. Boxplot showing the Tumor Immune Dysfunction and Exclusion (TIDE) scores in high- and low-ASRGL1 groups. C. Boxplot showing the expression of representative immune markers in high- and low-ASRGL1 groups. D. Gene Set Enrichment Analysis (GSEA) scores of immune cells in high- and low-ASRGL1 groups.

(**Figure 5A**, **5B**). Two core cytotoxic effector genes were downregulated in ASRGL1-high tumors: GZMB (log_2FC = -0.32, P < 0.001), PRF1 (log_2FC = -0.28, P < 0.001) (**Figure 5C**). ssGSEA enrichment scores of $CD8^+$ effector T cells (r_s = -0.23, FDR < 0.001) and NK cells (r_s = -0.18, FDR = 0.003) showed significant negative correlation with ASRGL1 expression (**Figure 5D**).

Cell-specific localization of ASRGL1 and intercellular communication of mast cell subsets

scRNA-seq feature plots showed ASRGL1 transcripts were mainly detected in mast cell cluster, with negligible expression in epithelial, T cell, fibroblast and endothelial populations (**Figure 6A**, **6B**). Mast cells were divided into $ASRGL1^+$ and $ASRGL1^-$ subsets based on transcript expression status. Cell-cell communication analysis (CellPhoneDB v3) calculated weighted outgoing ligand-receptor interaction strength: $ASRGL1^+$ mast cells had higher median interaction strength (2.17 vs. 1.39, Wilcoxon P < 0.001). The top enriched ligand-receptor axes included VEGF, LIFR, OSM and CSF signaling (**Figure 6C-E**). ssGSEA metabolic pathway analysis within mast cell subpopulations showed steroid biosynthesis pathway NES = 1.51

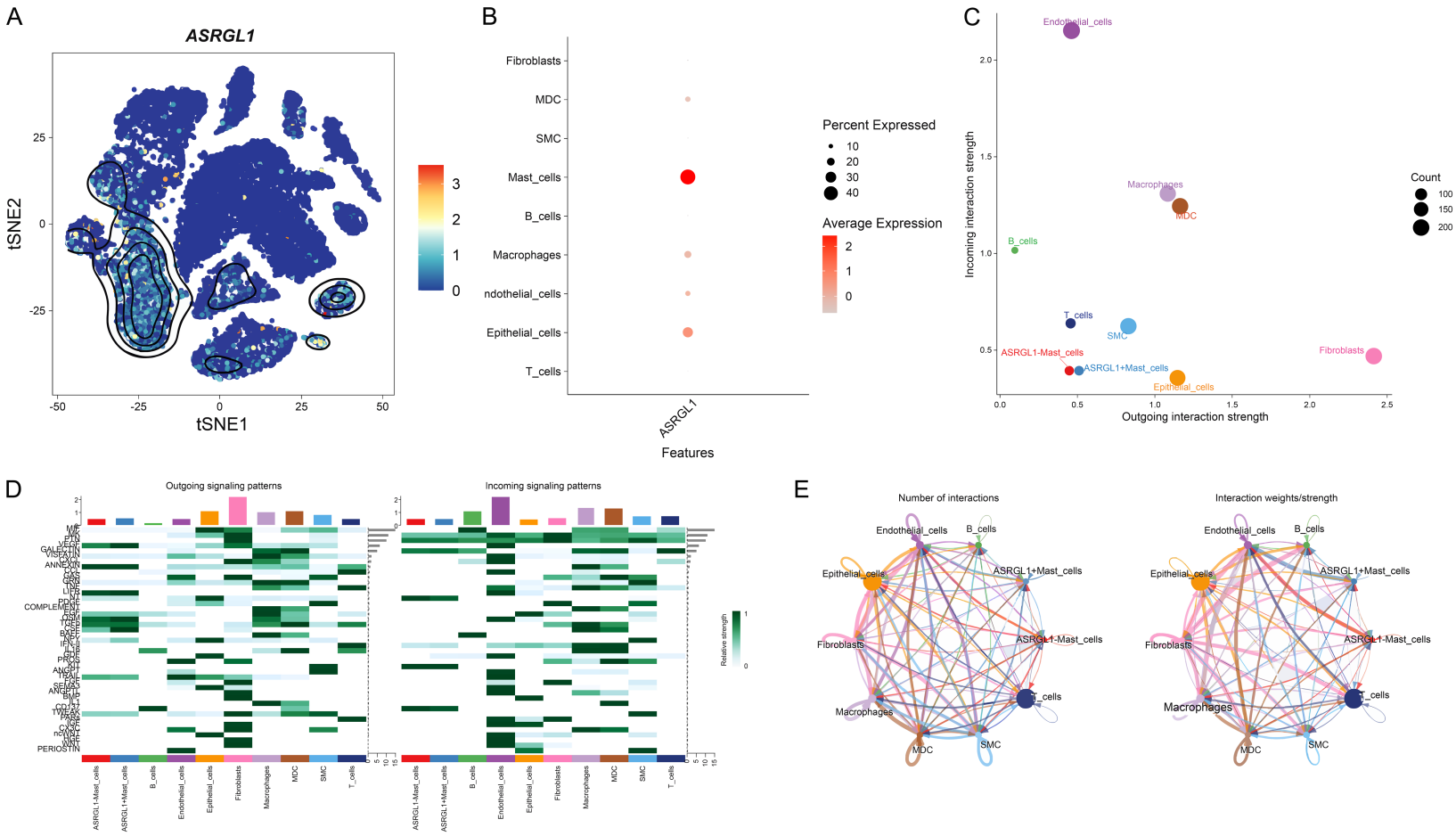


Figure 6. The expression of ASRGL1 in cell groups. A. Expression of ASRGL1 in t-SNE plot. B. Dot plot showing the expression of ASRGL1 in major cell types. C, D. Difference in interaction strength between ASRGL1-positive (ASRGL1$^+$) mast cells and ASRGL1-negative (ASRGL1$^-$) mast cells. E. Number of interactions and interaction weight/strength of ASRGL1-positive (ASRGL1$^+$) mast cells and ASRGL1-negative (ASRGL1$^-$) mast cells.

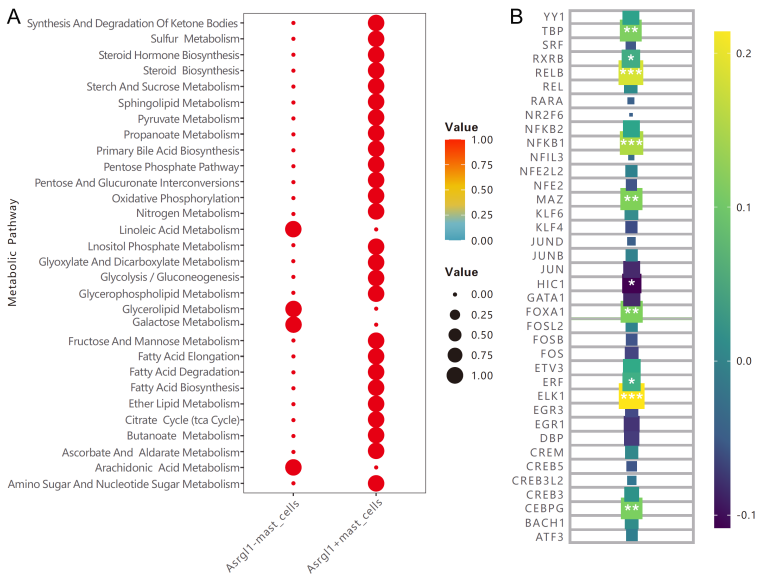


Figure 7. The biological characteristics for ASRGL1. A. Activity of metabolic pathways in ASRGL1-positive (ASRGL1$^+$) mast cells and ASRGL1-negative (ASRGL1$^-$) mast cells. B. Correlation between translation factors and ASRGL1.

(FDR = 0.016) in ASRGL1$^+$ mast cells. Spearman correlation within mast cell transcriptome revealed positive linear correlations between ASRGL1 and three transcription factors: ELK1 (r_s = 0.42, P < 0.001), RELB (r_s = 0.37, P < 0.001), NFKB1 (r_s = 0.34, P < 0.001) (**Figure 7A**, **7B**).

High-throughput screening of targeted compounds for ASRGL1-high PCa

To discern potential therapeutic agents exhibiting heightened sensitivity in patients with high ASRGL1 expression, we employed two distinct methodologies (**Figure 8A**). Our analyses leveraged drug response data derived from the Cancer Therapeutics Response Portal (CTRP) and the Profiling Relative Inhibition Simultaneously in Mixtures (PRISM) database. Initially, we conducted a comparative analysis of drug responses between cohorts exhibiting high ASRGL1 expression (top decile) and low ASRGL1 expression (bottom decile). This endeavor aimed to identify compounds demonstrating diminished estimated Area Under the Curve (AUC) values in the high ASRGL1 group (log_2FC > 0.10). Subsequently, Spearman correlation analysis between AUC values and Patient-derived Prognosis Score (PPS) was undertaken to discern compounds exhibiting a negative correlation coefficient (Spearman's r < -0.30 for CTRP or -0.35 for PRISM). These rigorous analyses culminated in the identification of five CTRP-derived compounds (including CR-1-31B, paclitaxel, SB-743921, leptomycin B, and panobinostat) and eight PRISM-derived compounds (including floxuridine, canertinib, AZD8931, pevonedistat, dacomitinib, tacalcitol, poziotinib, and SGI-1027). Notably, all identified compounds exhibited reduced estimated AUC values in the high PPS group and manifested a negative correlation with PPS (**Figure 8B** and **8C**).

Discussion

Our study, by integrating single-cell transcriptomic atlases, Mendelian randomisation analysis, clinical cohort verification, and drug sensitivity data, systematically investigates the pathological functions of ASRGL1 in PCa. First, we constructed a cell atlas of human prostatic tissue, revealing a significant expansion of mast cells, T cells and myeloid-dendritic cells within the PCa TME, suggesting their crucial roles in disease progression. Using MR for causal inference, we provide, for the first time, direct genetic evidence that elevated levels of the ASRGL1 protein constitute an independent risk factor for PCa (OR = 1.074, P < 0.001). The robustness of this causal association is strongly supported by the results of pleiotropy tests and leave-one-out sensitivity analysis, effectively mitigating potential confounding biases from individual dominant SNPs.

ASRGL1, a member of the asparaginase family with β-asparaginase activity, has been linked to tumor progression and patient outcomes in other cancers. Its overexpression is known to directly promote tumor cell proliferation and inhibit apoptosis [14]. For instance, in cervical cancer models, ASRGL1 knockdown led to reduced levels of cyclin-dependent kinase 2 (CDK2) and cyclin A2, causing significant cell cycle disruptions [15]. Similarly, in hepatocellular carcinoma, ASRGL1 knockdown increased p53 expression, decreased Cyclin B1 and CDK1 levels, induced G2/M phase arrest, and

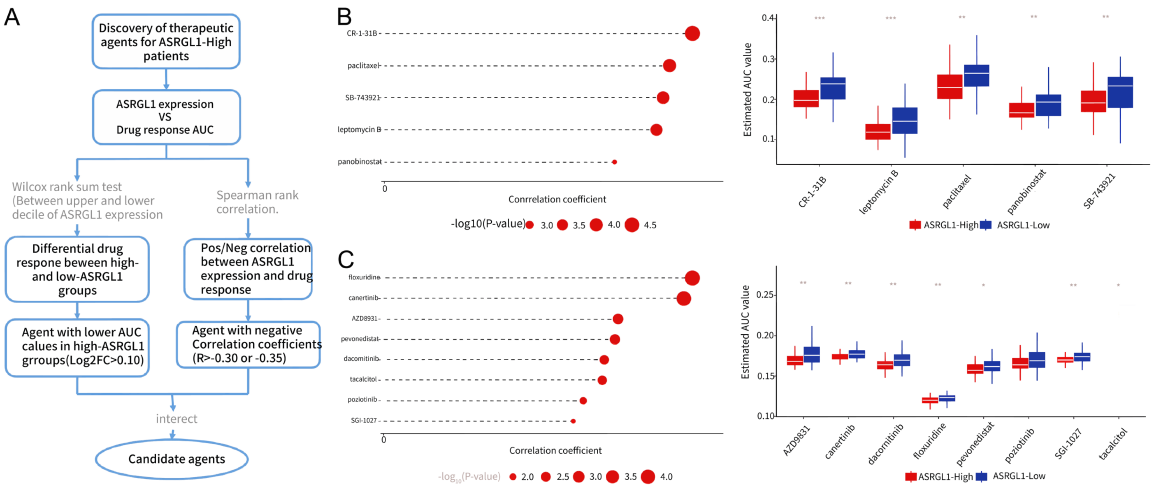


Figure 8. Drug response analysis. A. Schematic outlining the strategy to identify agents with higher drug sensitivity in high ASRGL1 patients. B. Results of Spearman's correlation analysis and differential drug response analysis of five Cancer Therapeutics Response Portal (CTRP)-derived compounds. C. Results of Spearman's correlation analysis and differential drug response analysis of eight Profiling Relative Inhibition Simultaneously in Mixtures (PRISM)-derived compounds. Note that lower values on the y-axis of boxplots imply greater drug sensitivity.

suppressed proliferation, migration, and invasion [14]. While these studies show variations in the specific cell cycle arrest phase, they collectively demonstrate ASRGL1's core oncogenic function: maintaining rapid cell-cycle progression by stabilizing key CDK-Cyclin proteins, thereby fueling tumor proliferation and malignancy. Our study aligns with and extends this understanding, confirming a significant correlation between ASRGL1 overexpression and poor prognosis in PCa, a relationship further substantiated by our MR analysis.

To investigate the mechanism underlying ASRGL1-driven PCa progression, we performed single-sample gene set enrichment analysis (ssGSEA). The results revealed that high ASRGL1 expression positively correlates with increased activity of the PI3K/AKT/mTOR signaling pathway, interferon response, G2M checkpoint, and notably, cholesterol homeostasis. We posit that this link to cholesterol metabolism is particularly significant. Dysregulated cholesterol homeostasis in PCa may theoretically provide abundant substrate for endogenous testosterone synthesis, potentially enabling tumors to bypass androgen deprivation therapy (ADT) and sustain androgen receptor (AR) signaling pathway activation [16, 17]. Therefore, we propose that ASRGL1-mediated dysregulation of cholesterol homeostasis represents a key mechanism promoting both tumor progression and endocrine therapy resistance, offering a novel perspective on its oncogenic function.

Given prior evidence linking ASRGL1 overexpression to alterations in the TME and immune cell infiltration in other cancers [18], we performed detailed immune profiling. Our analysis indicates that high ASRGL1 expression induces complex, functionally suppressive changes in the TME. Specifically, ASRGL1 overexpression was associated with marked upregulation of the immune checkpoint molecule CD276 (B7-H3) and suppression of CD28/CD40 co-stimulatory signaling, collectively appearing to impair T cell-mediated anti-tumor immunity. Furthermore, key NK cell functional molecules (CD244, CD48) were downregulated, likely dampening cytotoxic activity. Elevated levels of Neuropilin-1 (NRP1) alongside suppressed TNFSF15 may synergistically enhance tumor angiogenesis [19]. Interestingly, while the ESTIMATE Stromal score was decreased in the ASRGL1-high group, the immune score did not show a significant reduction. This suggests that ASRGL1 may not globally reduce immune infiltration but rather primarily suppresses the effector functions of key immune cells, including memory T cells, effector T cell and NK cells, thereby sculpting a profoundly immunosuppressive TME. This overall immunosuppressive state may be a critical driver of PCa progression and therapy resistance. Consequently, targeting ASRGL1 or its downstream effects (e.g.,

on CD276, NRP1), represents a promising avenue for exploration in PCa immunotherapy.

Mast cells are integral yet complex components of the TME, with conflicting roles reported in PCa progression [20-24]. Our scRNA-seq analysis revealed that ASRGL1 expression is predominantly enriched in the mast cell population. We subsequently stratified mast cells into ASRGL1$^+$ and ASRGL1$^-$ functional subsets. Notably, ASRGL1$^+$ mast cells exhibited significantly enhanced outgoing interaction strength, primarily involving VEGF, LIFR, oncostatin M (OSM), and CSF signaling pathway. Mechanistically, OSM binding to its receptor OSMR activates the JAK-STAT3 pathway [25], and can upregulate VEGF expression through PI3K-Akt, ERK1/2 MAPK, and JAK-STAT signaling, thereby promoting angiogenesis and tumor growth [26]. Our data support a model wherein the ASRGL1$^+$ MC subset likely drives PCa progression through an OSM-VEGF axis-mediated pro-angiogenic phenotype. First, a higher proportion of ASRGL1$^+$ cells corresponded to greater activations of PI3K-Akt and JAK-STAT signal pathways. Second, the MAPK pathway, activated downstream of OSM signaling, can induce phosphorylation of the transcription factor Elk-1, a known regulator of VEGF [27]. Finally, cell-cell interaction analysis demonstrated significantly enhanced communication between ASRGL1$^+$ mast cells and endothelial cells, further corroborating the pro-angiogenic functional role of this subset.

In addition, the NF-κB family transcription factors RELB and NFKB1 (p105/p50) showed relatively high expression in ASRGL1$^+$ mast cells. RELB, a key component of the non-canonical NF-κB pathway, can promote PCa progression under androgen-deprivation conditions by activating AR splice variants such as AR-V7 and upregulating PD-L1/PD-1 to induce immunosuppression [28-30]. NFKB1, primarily acting through the canonical NF-κB pathway, can dimerize with RELA (p65) to activate pro-survival (e.g., Bcl-2) and inflammatory (e.g., IL-6, IL-8) genes, fostering an inflammatory microenvironment conducive to CRPC progression [31]. The enrichment of these factors in ASRGL1$^+$ mast cells suggests a potential role for this subset in promoting therapy resistance.

Our drug sensitivity analysis identified five compounds from the CTRP database (e.g., panobinostat, paclitaxel) and eight from the PRISM database (e.g., pevonedistat, floxuridine) as potential therapeutics for ASRGL1-high PCa. Importantly, the targets and mechanisms of these compounds (e.g., histone deacetylase inhibition, cell cycle disruption, nucleotide metabolism interference) exhibit high concordance with ASRGL1's implicated oncogenic functions - such as epigenetic regulation, cell cycle progression, and metabolic reprogramming. This congruence provides a solid mechanistic rationale for their therapeutic efficacy in ASRGL1-high PCa and highlights promising candidates for further experimental validation.

A key novel insight of our study is the specific enrichment of ASRGL1 in mast cells within the PCa TME. While previous studies linked ASRGL1 to tumor cell-autonomous proliferation in other cancer [14, 15], our single-cell resolution analysis suggests a paradigm shift: ASRGL1 may exert its oncogenic effects significantly through modulating stromal-immune crosstalk. We hypothesize that ASRGL1-high mast cells act as "orchestrators" of an immunosuppressive and pro-angiogenic niche. The observed upregulation of OSM and VEGF pathways in these cells, coupled with their enhanced communication with endothelial cells and the associated immunosuppressive landscape, likely facilitates tumor growth and therapy resistance by inhibiting effective anti-tumor immunity. This perspective underscores the therapeutic potential of targeting stromal components like ASRGL1$^+$ mast cells to remodel the TME, moving beyond a sole focus on epithelial tumor cells.

Our study has several limitations. Firstly, the analyses are primarily based on computational interrogation of public databases. Secondly, our conclusions, particularly the proposed mechanistic roles of ASRGL1 in mast cells and cholesterol metabolism, require direct experimental validation using in vitro and in vivo models. Future studies should employ genetic manipulation in mast cells and prostate cancer models to definitively establish causality and elucidate the precise molecular mechanisms.

Conclusion

In summary, our multi-omics investigation identifies ASRGL1 as a novel oncogene in prostate cancer, with elevated expression causally

linked to increased disease risk and associated with a poorer prognosis. We propose that ASRGL1 contributes to PCa progression through multiple interconnected mechanisms: by potentially dysregulating cholesterol homeostasis to fuel therapy resistance, by orchestrating an immunosuppressive TME via mast cells, and by promoting a pro-angiogenic niche. These findings not only position ASRGL1 as a promising prognostic indicator but also reveal its role within the stromal-immune axis, offering fresh perspectives and potential therapeutic targets for the treatment of prostate cancer.

Disclosure of conflict of interest

None.

Address correspondence to: Guizhong Li, Department of Urology, Beijing Jishuitan Hospital, Capital Medical University, No. 31 Xinjiekou East Street, Xicheng District, Beijing 100035, China. E-mail: lee_gz99@163.com; Zheng Chen, Department of Urology, The First Affiliated Hospital of Jinan University, No. 613 Huangpu Avenue West, Tianhe District, Guangzhou 510630, Guangdong, China. E-mail: chenzh59@mail2.sysu.edu.cn

References

[1] Bray F, Laversanne M, Sung H, Ferlay J, Siegel RL, Soerjomataram I and Jemal A. Global cancer statistics 2022: GLOBOCAN estimates of incidence and mortality worldwide for 36 cancers in 185 countries. CA Cancer J Clin 2024; 74: 229-263.

[2] Chu F, Chen L, Guan Q, Chen Z, Ji Q, Ma Y, Ji J, Sun M, Huang T, Song H, Zhou H, Lin X and Zheng Y. Global burden of prostate cancer: age-period-cohort analysis from 1990 to 2021 and projections until 2040. World J Surg Oncol 2025; 23: 98.

[3] James ND, Tannock I, N'Dow J, Feng F, Gillessen S, Ali SA, Trujillo B, Al-Lazikani B, Attard G, Bray F, Compérat E, Eeles R, Fatiregun O, Grist E, Halabi S, Haran Á, Herchenhorn D, Hofman MS, Jalloh M, Loeb S, MacNair A, Mahal B, Mendes L, Moghul M, Moore C, Morgans A, Morris M, Murphy D, Murthy V, Nguyen PL, Padhani A, Parker C, Rush H, Sculpher M, Soule H, Sydes MR, Tilki D, Tunariu N, Villanti P and Xie LP. The Lancet Commission on prostate cancer: planning for the surge in cases. Lancet 2024; 403: 1683-1722.

[4] Schröder FH, Hugosson J, Roobol MJ, Tammela TL, Zappa M, Nelen V, Kwiatkowski M, Lujan M, Määttänen L, Lilja H, Denis LJ, Recker F, Paez A, Bangma CH, Carlsson S, Puliti D, Villers A, Rebillard X, Hakama M, Stenman UH, Kujala P, Taari K, Aus G, Huber A, van der Kwast TH, van Schaik RH, de Koning HJ, Moss SM and Auvinen A; ERSPC Investigators. Screening and prostate cancer mortality: results of the European randomised study of screening for prostate cancer (ERSPC) at 13 years of follow-up. Lancet 2014; 384: 2027-2035.

[5] Raychaudhuri R, Lin DW and Montgomery RB. Prostate cancer: a review. JAMA 2025; 333: 1433-1446.

[6] Farashi S, Kryza T, Clements J and Batra J. Post-GWAS in prostate cancer: from genetic association to biological contribution. Nat Rev Cancer 2019; 19: 46-59.

[7] Chen L, Xu YX, Wang YS, Ren YY, Dong XM, Wu P, Xie T, Zhang Q and Zhou JL. Prostate cancer microenvironment: multidimensional regulation of immune cells, vascular system, stromal cells, and microbiota. Mol Cancer 2024; 23: 229.

[8] Falagario UG, Abbadi A, Remmers S, Björnebo L, Bogdanovic D, Martini A, Valdman A, Carrieri G, Menon M, Akre O, Eklund M, Nordström T, Grönberg H, Lantz A and Wiklund P. Biochemical recurrence and risk of mortality following radiotherapy or radical prostatectomy. JAMA Netw Open 2023; 6: e2332900.

[9] Freedland SJ, Humphreys EB, Mangold LA, Eisenberger M, Dorey FJ, Walsh PC and Partin AW. Risk of prostate cancer-specific mortality following biochemical recurrence after radical prostatectomy. JAMA 2005; 294: 433-439.

[10] Antonarakis ES, Lu C, Wang H, Luber B, Nakazawa M, Roeser JC, Chen Y, Mohammad TA, Chen Y, Fedor HL, Lotan TL, Zheng Q, De Marzo AM, Isaacs JT, Isaacs WB, Nadal R, Paller CJ, Denmeade SR, Carducci MA, Eisenberger MA and Luo J. AR-V7 and resistance to enzalutamide and abiraterone in prostate cancer. N Engl J Med 2014; 371: 1028-1038.

[11] Pungsrinont T, Kallenbach J and Baniahmad A. Role of PI3K-AKT-mTOR pathway as a pro-survival signaling and resistance-mediating mechanism to therapy of prostate cancer. Int J Mol Sci 2021; 22: 11088.

[12] Liu D, Wang L and Guo Y. Advances in and prospects of immunotherapy for prostate cancer. Cancer Lett 2024; 601: 217155.

[13] Emdin CA, Khera AV and Kathiresan S. Mendelian randomization. JAMA 2017; 318: 1925-1926.

[14] Wang X, Wang Y, Yang L, Yuan J, Shen W, Zhang W, Wang J and Tao K. ASRGL1 downregulation suppresses hepatocellular carcinoma tumorigenesis in a CDK1-dependent manner. Dig Liver Dis 2023; 55: 955-966.

[15] Lv XF, Hong HQ, Liu L, Cui SH, Ren CC, Li HY, Zhang XA, Zhang LD, Wei TX, Liu JJ, Xing WY, Fu H and Yan SJ. RNAi-mediated downregulation of asparaginase-like protein 1 inhibits growth and promotes apoptosis of human cervical cancer line SiHa. Mol Med Rep 2018; 18: 931-937.

[16] Gordon JA, Noble JW, Midha A, Derakhshan F, Wang G, Adomat HH, Tomlinson Guns ES, Lin YY, Ren S, Collins CC, Nelson PS, Morrissey C, Wasan KM and Cox ME. Upregulation of scavenger receptor B1 is required for steroidogenic and nonsteroidogenic cholesterol metabolism in prostate cancer. Cancer Res 2019; 79: 3320-3331.

[17] Jeon JC, Park J, Park S, Moon KH, Cheon SH and Park S. Hypercholesterolemia is associated with a shorter time to castration-resistant prostate cancer in patients who have undergone androgen deprivation therapy. World J Mens Health 2016; 34: 28-33.

[18] Xue C, Gao P, Cui X, Zhang X, Lei J, Li R, Zhu C and Qin X. ASRGL1 correlates with immune cell infiltration in hepatocellular carcinoma and can serve as a prognostic biomarker. Front Oncol 2021; 11: 680070.

[19] Kim YJ, Bae J, Shin TH, Kang SH, Jeong M, Han Y, Park JH, Kim SK and Kim YS. Immunoglobulin Fc-fused, neuropilin-1-specific peptide shows efficient tumor tissue penetration and inhibits tumor growth via anti-angiogenesis. J Control Release 2015; 216: 56-68.

[20] Khazaie K, Blatner NR, Khan MW, Gounari F, Gounaris E, Dennis K, Bonertz A, Tsai FN, Strouch MJ, Cheon E, Phillips JD, Beckhove P and Bentrem DJ. The significant role of mast cells in cancer. Cancer Metastasis Rev 2011; 30: 45-60.

[21] Maltby S, Khazaie K and McNagny KM. Mast cells in tumor growth: angiogenesis, tissue remodelling and immune-modulation. Biochim Biophys Acta 2009; 1796: 19-26.

[22] Pittoni P and Colombo MP. The dark side of mast cell-targeted therapy in prostate cancer. Cancer Res 2012; 72: 831-835.

[23] Hempel HA, Cuka NS, Kulac I, Barber JR, Cornish TC, Platz EA, De Marzo AM and Sfanos KS. Low intratumoral mast cells are associated with a higher risk of prostate cancer recurrence. Prostate 2017; 77: 412-424.

[24] Nonomura N, Takayama H, Nishimura K, Oka D, Nakai Y, Shiba M, Tsujimura A, Nakayama M, Aozasa K and Okuyama A. Decreased number of mast cells infiltrating into needle biopsy specimens leads to a better prognosis of prostate cancer. Br J Cancer 2007; 97: 952-956.

[25] Geethadevi A, Nair A, Parashar D, Ku Z, Xiong W, Deng H, Li Y, George J, McAllister DM, Sun Y, Kadamberi IP, Gupta P, Dwinell MB, Bradley WH, Rader JS, Rui H, Schwabe RF, Zhang N, Pradeep S, An Z and Chaluvally-Raghavan P. Oncostatin M receptor-targeted antibodies suppress STAT3 signaling and inhibit ovarian cancer growth. Cancer Res 2021; 81: 5336-5352.

[26] Demyanets S, Kaun C, Rychli K, Pfaffenberger S, Kastl SP, Hohensinner PJ, Rega G, Katsaros KM, Afonyushkin T, Bochkov VN, Paireder M, Huk I, Maurer G, Huber K and Wojta J. Oncostatin M-enhanced vascular endothelial growth factor expression in human vascular smooth muscle cells involves PI3K-, p38 MAPK-, Erk1/2- and STAT1/STAT3-dependent pathways and is attenuated by interferon-γ. Basic Res Cardiol 2011; 106: 217-231.

[27] Xu L, Fukumura D and Jain RK. Acidic extracellular pH induces vascular endothelial growth factor (VEGF) in human glioblastoma cells via ERK1/2 MAPK signaling pathway: mechanism of low pH-induced VEGF. J Biol Chem 2002; 277: 11368-11374.

[28] Nadiminty N, Dutt S, Tepper C and Gao AC. Microarray analysis reveals potential target genes of NF-kappaB2/p52 in LNCaP prostate cancer cells. Prostate 2010; 70: 276-287.

[29] Mehraein-Ghomi F, Church DR, Schreiber CL, Weichmann AM, Basu HS and Wilding G. Inhibitor of p52 NF-κB subunit and androgen receptor (AR) interaction reduces growth of human prostate cancer cells by abrogating nuclear translocation of p52 and phosphorylated AR (ser81). Genes Cancer 2015; 6: 428-444.

[30] Zhang Y, Zhu S, Du Y, Xu F, Sun W, Xu Z, Wang X, Qian P, Zhang Q, Feng J and Xu Y. RelB upregulates PD-L1 and exacerbates prostate cancer immune evasion. J Exp Clin Cancer Res 2022; 41: 66.

[31] Wang X, Fang Y, Sun W, Xu Z, Zhang Y, Wei X, Ding X and Xu Y. Endocrinotherapy resistance of prostate and breast cancer: importance of the NF-κB pathway (Review). Int J Oncol 2020; 56: 1064-1074.